Modeling of intensity-modulated focused ultrasound in pediatric brain tumors using acoustic holograms

Sergio Jiménez-Gambín[†*], Antonios N. Pouliopoulos[‡], Zachary K. Englander[§], Noé Jiménez[†], Francisco Camarena[†], Elisa E. Konofagou[‡,¶], Stergios Zacharoulis[‖] and Cheng-Chia Wu[**,††]
[†]Instituto de Instrumentación para Imagen Molecular, Universitat Politècnica de València - CSIC, Valencia, Spain
Departments of [‡]Biomedical Engineering, [¶]Radiology, Columbia University, New York City, USA
Departments of [§]Neurological Surgery, [‖]Pediatrics, [**]Radiation Oncology, Columbia University Irving Medical Center, New York City, USA
[††]Herbert Irving Comprehensive Cancer Center, New York City, USA
[*]Email: serjigam@upv.es

2021 IEEE International Ultrasonics Symposium (IUS) | 978-1-6654-0355-9/21/$31.00 ©2021 IEEE | DOI: 10.1109/IUS52206.2021.9593797

***Abstract*—Targeted drug delivery to enhance chemotherapy treatments in brain tumors can be achieved by opening the blood-brain barrier in a non-invasive, transient, localized, safe manner by using focused ultrasound (FUS) and microbubbles. However, as brain tumors are large and irregular structures, conventional single-element FUS methods are inefficient because they do not allow large covering. In this study, we numerically showed how 3D-printed acoustic holograms allow to correct the skull aberrations and to produce a large and localized focusing along a pediatric brain tumor. Several targeting configurations were numerically studied aiming to increase the covered tumor volume while reducing the off-target coverage. Fluid-like tissue simulations were performed using the k-space method. We used a 250-kHz single-element device in different configurations (ROC=110 mm, OD=110 or 132 mm, ID=0 or 44 mm), where the optimal setup with lens (OD=132 mm, ID=0 mm) provided a 16 % of tumor coverage compared to the 5 % obtained using the transducer without lens (OD=110 mm, ID=44 mm), while keeping a reduced 0.06 % of off-target coverage. The focal amplitude decreases 1.6 times accordingly to the focus spread. The estimated sonication duration and the number of microbubble injections can be reduced by 3.2 times, defining a time- and cost-efficient approach. The reported approach is simple, low-cost, and feasible to offering personalized, tumor-directed precision FUS treatment, to improve drug delivery for pediatric patients with brain tumors.**

***Index Terms*—acoustic hologram, blood-brain barrier opening, brain tumor**

I. Introduction

Diffuse midline glioma (DMG) - H3K27M-mutant [1], is the most aggressive primary pediatric brain tumor. It is very infiltrative and is frequently located in the pons within the brainstem, a very delicate region vital for survival. To date, there is no effective treatment and the median overall survival is less than 1 year with radiation therapy. On the one hand, conventional surgical resection is not possible in most cases due to the tumor location. On the other hand, the BBB prevents most therapeutic drugs from crossing into the brain parenchyma and they can not reach the target cancerous cells [2].

Different approaches have been assessed in previous works to treat primary brain tumors. Some of them by disrupting the BBB [3], [4], and others by direct injection of drugs into the brain using convection enhanced delivery [5]–[7]. However, these techniques have not been widely used due to difficulties related to their routine implementation in the clinic. An alternative approach is using microbubble-enhanced FUS to increase the permeability of the BBB in a non-invasive, localized, transient, and safe manner, which has been successfully demonstrated in small and large animals and preclinical glioma models. However, the transcranial FUS propagation is complex because the skull is an irregular and thick bone layer that distorts and attenuates the beam leading to undesired effects [8]. Besides, conventional FUS systems lack a large tumor coverage. Nevertheless, a recent technology using acoustic holograms can partially address these limitations [9].

In this study, we assessed the feasibility and capabilities of acoustic holograms coupled to a 250 kHz single-element FUS transducer [10] to increase the targeted volume of a pediatric cancer brain tumor. These lenses allow to correct the skull aberrations and generate a focal shape matching the geometry of the tumor, thus improving the performance compared with conventional single-element transducers. Different lens designs were studied, and the results indicated that the larger tumor coverage with a reduced off-target dispersion was obtained with the curved-slice-hologram configuration, where the single-element FUS transducer had an outer diameter aperture of 132 mm, a radius of curvature of 110 mm, and no central void, providing coverage of the 15.9 % of the tumor.

This research has been supported by the Spanish Ministry of Science, Innovation and Universities through grants "Juan de la Cierva - Incorporación" (IJC2018-037897-I) and PID2019111436RB-C22, by the Agència Valenciana de la Innovació through grant INNVAL10/19/016 and INNCON/2021/8, by Generalitat Valenciana through grants ACIF/2017/045 and BEFPI/2019/075, by the National Institutes of Health through grants 5R01EB009041 and 5R01AG038961, by the Gary and Yael Fegel Family Foundation, Matheson Foundation (UR010590), St. Baldrick's Foundation, Star and Storm Foundation, the Herbert Irving Cancer Center Support Grant (P30CA013696), and the Herbert Irving Cancer Center CAPRI Grant (NIH R38CA231577-01). Action co-financed by the Programa Operativo del Fondo Europeo de Desarrollo Regional (FEDER) of the Comunitat Valenciana (IDIFEDER/2021/004) and Comunitat Valenciana 2014-2020 (IDIFEDER/2018/022).

978-0-7381-1209-1/21/$31.00 ©2021 IEEE

Authorized licensed use limited to: UNIVERSIDAD POLITECNICA DE VALENCIA. Downloaded on November 30,2021 at 14:05:17 UTC from IEEE Xplore. Restrictions apply.

II. Materials and methods

For this numerical study, we acquired the 3D geometry and acoustical properties of a pediatric skull from X-ray CT images, and we identified the target tumor structure (DMG - H3K27M-mutant) from MRI. Then, we used the single-element FUS transducer (H-231 Sonic Concepts, f_0=0.25 MHz, OD=110 mm, F=110 mm, and ID=44 mm) in FDA-approved phase I clinical trials (NCT04118764 and NCT04804709) positioned towards the tumor through the occipital/parietal skull area. An acoustic lens was designed and coupled to it. Finally, the pressure-field distribution was simulated.

A. Numerical simulation

We selected the pseudo-spectral simulation method with k-space dispersion correction implemented in the k-Wave toolbox [15], [16] for Matlab. We used a numerical grid with a spatial step of $\Delta x = \Delta y = \Delta z = 1$ mm and a numerical temporal step of $\Delta t = 57.7$ ns, leading to a Courant-Friedrichs-Lewy number of 0.2 and a spatial sampling of 6 grid points per wavelength in soft tissue at f_0.

B. CT and MRI acquisition

We used a CT-scan from a human pediatric head to model the skull geometry, with a slice thickness of 2 mm and in-slice pixel size of 1×1 mm. The heterogeneous density and sound speed were converted from Hounsfield units using the linear-piecewise polynomials proposed in [11], [12]. The skull absorption was set to 1.5 dB/cm at f_0 [13]. After, we segmented the tumor from the MRI using the ITK-SNAP software [14], with an original resolution of $0.4 \times 0.4 \times 4.4$ mm. This tumor represents a 2.7 % of the whole brain ($V_{tumor} = 31.1$ cm^3 compared to $V_{brain} = 1132.4$ cm^3). Acoustical properties of the brain were also simulated for better accuracy, using a sound speed of $c_{brain} = 1560$ m/s, a density of $\rho_{brain} = 1000$ kg/m^3, and an absorption of 0.10 dB/cm at f_0 [13].

C. Lens design

The distribution of heights along the lens surface was obtained by analyzing the complex-conjugate of the holographic wavefront, i.e., the pressure-field recorded at a curved and parallel surface to the transducer surface [9]. A set of virtual sources along a slice of the tumor were used for the back-propagation step. The lens was made of a 3D-printable resin from Formlabs (ClearResin material, $c_L = 2580$ m/s, $\rho_L = 1171$ kg/m^3, $\alpha = 0.69$ dB/cm at f_0).

D. Quality parameter evaluation

First, we defined V_{in} as the tumor volume covered by the active beam. The higher V_{in} is, the higher the coverage of the tumor is, and the more efficient and localized the treatment is. Second, we defined V_{out} as the off-target volume (healthy brain volume) covered by the active beam. The smaller V_{out} is, the less off-target coverage, and the more localized the treatment is. Third, we defined $RAR = A_{lens}/A_{transducer}$ (Relative focal Amplitude Reduction) to assess the pressure reduction at the maximum of the focus A_{lens} using a lens transcranially, compared with the transcranial focal amplitude $A_{transducer}$ provided by the H-231 transducer without the lens. This parameter is related to the ratio between focal pressures and off-target pressures. Therefore, considering the initial low-gain of the H-231 transducer and the focus spreading due to the lens (low A_{lens}), a high ratio between focal and off-target pressures is required to avoid that a slight over- or under-estimation in the skull attenuation prediction leads to an undesired large or inexistent BBB opening, respectively. Although one can amplify the applied input signal, the skull attenuation estimation accuracy is critical for a successful BBB opening. However, treatment planning could account for the differences in RAR across patients. The interest in using acoustic holograms lies in achieving a higher V_{in} than the H-231 transducer without lens, while keeping a reduced V_{out}.

III. Results

Four configurations to assess the focusing quality were evaluated, starting with the H-231 transducer without lens, then coupling a lens to it, afterwards using a lens coupled to a transducer similar to the H-231 but with higher aperture, and finally using a lens coupled to the higher aperture transducer and without the central void to increase the total active radiating surface. We targeted the tumor through the skull's occipital region according to the focal length of the transducer. Note that this transducer's position is fixed in all configurations.

A. FUS transducer

The pressure-field distribution using the conventional H-231 single-element FUS transducer is shown in Fig. 1, where a clear focused beam at the center of the tumor is observed. This case provides $V_{in} = 1.5$ cm^3, which corresponds to 4.9 % of the total tumor volume, and $V_{out} = 0.2$ cm^3, representing 0.6 % of the total tumor volume. This transducer has a transcranial linear focal gain of $G = 7.4$. The focal volume shown in red in Fig. 1 (d) is obtained by thresholding the resulting pressure field between the maximum pressure value found in the tumor p_0 and the decay at its half (i.e., the FWHM). The BBB is expected to be opened with great accuracy within this focal region.

B. FUS transducer with lens

The results of coupling a lens to the H-231 transducer are shown in Fig. 2, where a complex-shape and broad focus along the tumor is observed. This approach provides a $V_{in} = 3.9$ cm^3, representing 12.4 % of the total tumor volume and 2.5 times greater than in the previous case without lens. Then, $V_{out} = 1.9$ cm^3, representing 6.2 % of the total tumor volume, around 10 times greater than in the conventional case. However, this value for V_{out} is small compared to the size of the whole brain (0.17 % of it). Finally, $RAR = 0.42$, thus we have to be 2.4 times ($1/RAR$) more accurate in the skull attenuation prediction for a successful BBB opening at the focal region. As expected, RAR decreases because the lens is defocusing the acoustic energy along the tumor.

Authorized licensed use limited to: UNIVERSIDAD POLITECNICA DE VALENCIA. Downloaded on November 30,2021 at 14:05:17 UTC from IEEE Xplore. Restrictions apply.

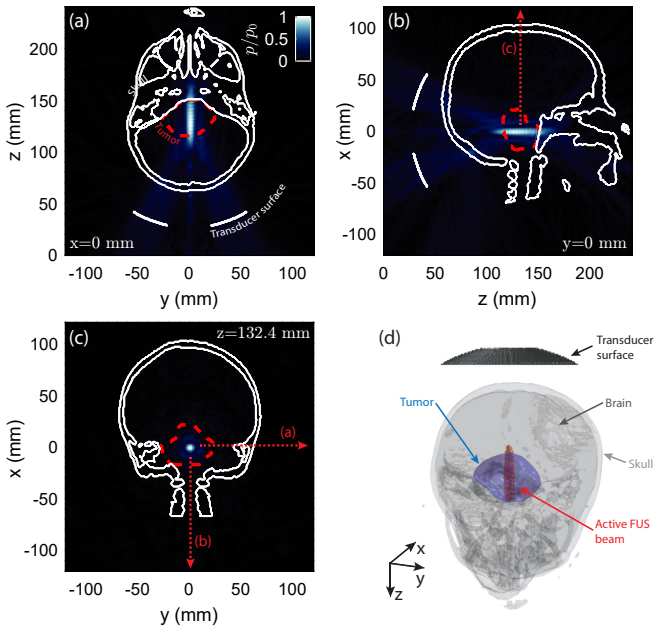


Fig. 1. Pressure-field distribution using the H-231 transducer normalized to p_0. (a) Axial plane at $x = 0$ mm. (b) Sagittal plane at $y = 0$ mm. (c) Coronal plane at $z = 132.4$ mm. (d) 3D view.

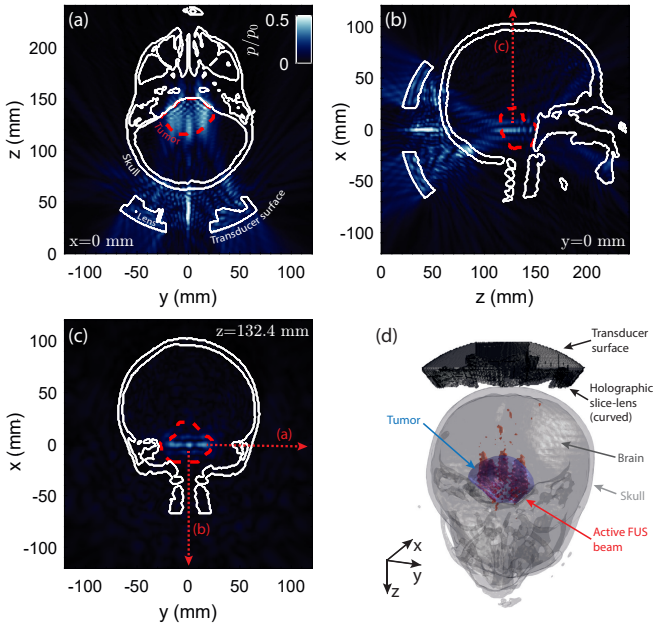


Fig. 3. Pressure-field distribution normalized to p_0 using the lens coupled to the higher-aperture transducer. (a) Axial plane at $x = 0$ mm. (b) Sagittal plane at $y = 0$ mm. (c) Coronal plane at $z = 132.4$ mm. (d) 3D view.

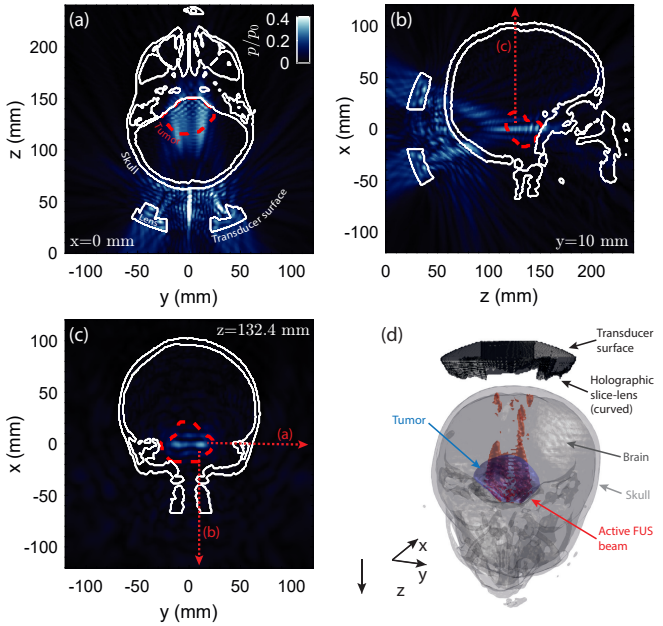


Fig. 2. Pressure-field distribution normalized to p_0 using the lens coupled to the transducer. (a) Axial plane at $x = 0$ mm. (b) Sagittal plane at $y = 10$ mm. (c) Coronal plane at $z = 132.4$ mm. (d) 3D view.

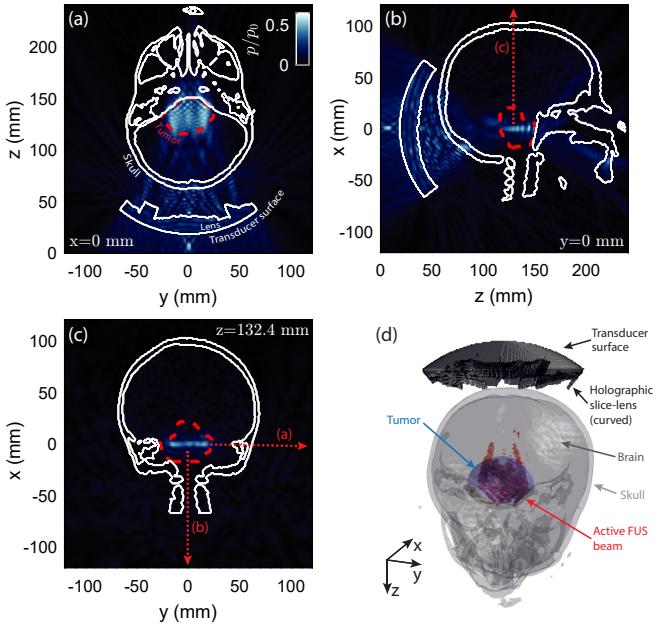


Fig. 4. Pressure-field distribution normalized to p_0 using the lens coupled to the higher- and complete-aperture transducer (no central void). (a) Axial plane at $x = 0$ mm. (b) Sagittal plane at $y = 0$ mm. (c) Coronal plane at $z = 132.4$ mm. (d) 3D view.

Authorized licensed use limited to: UNIVERSIDAD POLITECNICA DE VALENCIA. Downloaded on November 30,2021 at 14:05:17 UTC from IEEE Xplore. Restrictions apply.

C. Larger aperture FUS transducer with lens

The aperture of the H-231 transducer was chosen to allow for sufficient contact area with human skulls. However, at a frequency of 0.25 MHz, the reduced aperture is a limiting factor to provide a considerable focusing quality improvement, as the results showed a good but not uniform FUS coverage along the tumor. Therefore, we increased the transducer aperture from $2a = 110$ mm to $2a = 132$ mm. The results are shown in Fig. 3. The FUS covers the entire slice of the tumor with great accuracy while reducing the off-target coverage. This approach provides a $V_{in} = 3.9$ cm^3, similar to previous case. Then, $V_{out} = 0.8$ cm^3, around 4 times greater than in the case without lens and about a half lower than previous case, considerably reducing the off-target coverage. Finally, $RAR = 0.54$, improving previous case. Thereby, this approach shows a great performance.

D. No central void, larger aperture FUS transducer with lens

Assuming that the passive cavitation detector could be positioned confocally but outside the spherical section of the transducer, this additional central surface could be used to increase the active aperture. For this approach, we kept the aperture to $2a = 132$ mm, but without void. Fig. 4 shows a high-quality, complex broad focus along the slice of the tumor. The focus shows an excellent in-target pressure homogeneity and a sharp difference between focal and off-target pressure regions [see Fig. 4 (a,b,c)]. This approach provides $V_{in} = 4.9$ cm^3, representing 15.9 % of the total tumor volume, and 3.3 times higher than in the conventional case. Then, $V_{out} = 0.7$ cm^3, around 3.7 times greater than in the conventional case and around 13 % lower than in the previous case. In addition, $RAR = 0.64$, which implies a considerable improvement. This approach shows the best performance, albeit at the expense of having no concentric passive cavitation detection device.

IV. Conclusion

The reported results showed that all approaches using a lens coupled to the FUS transducer can improve the covered tumor volume. The covered off-target volume also increased, although it was a small volume relative to the entire brain volume. However, the focal gain was reduced about a half in all the cases, which is a relevant disadvantage as the original gain of the H-231 transducer was already low. Nevertheless, the low ultrasound attenuation of a pediatric skull in addition to the low working frequency, both leading to minimal aberration effects, would help to overcome the skull attenuation uncertainties and provide a high-quality focusing.

The most suitable holographic approach to ensure a large tumor coverage with low off-target coverage is the lens coupled to a transducer with OD=132 mm, ROC=110 mm, and no central void, resulting in a coverage of 15.9 % of the entire tumor by using a single sonication.

There is a lot of excitement surrounding the use of FUS in pediatric patients with DMG. This includes the phase I clinical trial, non-invasive FUS with oral panobinostat in children with progressive DMG (NCT04804709). The use of acoustic holograms for intensity-modulated FUS delivery to improve the coverage of pediatric brain tumors for BBB opening treatments is promising, and, may define a new path to overcome the difficulties of treating these tumors in these delicate-locations in the brain.

References

[1] Louis, D. N., Perry, A., Reifenberger, G., Von Deimling, A., Figarella-Branger, D., Cavenee, W. K., ... and Ellison, D. W., "The 2016 World Health Organization classification of tumors of the central nervous system: a summary," Acta neuropathologica, vol. 131, no. 6, pp. 803–820, 2016.

[2] Arvanitis, Costas D., Gino B. Ferraro, and Rakesh K. Jain. "The blood–brain barrier and blood–tumour barrier in brain tumours and metastases," Nature Reviews Cancer, vol. 20, no. 1, pp. 26–41, 2020.

[3] Groothuis, Dennis R. "The blood-brain and blood–tumor barriers: a review of strategies for increasing drug delivery," Neuro–oncology, vol 2, no. 1, pp. 45–59, 2000.

[4] Prados, M. D., Schold Jr, S. C., Fine, H. A., Jaeckle, K., Hochberg, F., Mechtler, L., ... and Graney, W., "A randomized, double–blind, placebo–controlled, phase 2 study of RMP–7 in combination with carboplatin administered intravenously for the treatment of recurrent malignant glioma," Neuro–oncology, vol 5(2), pp. 96–103, 2003.

[5] Boiardi, A., Silvani, A., Eoli, M., Lamperti, E., Salmaggi, A., Gaviani, P., ... and Broggi, G., "Treatment of recurrent glioblastoma: can local delivery of mitoxantrone improve survival?," Journal of neuro–oncology, vol 88, no. 1, pp. 105–113, 2008.

[6] Bruce, J. N., Fine, R. L., Canoll, P., Yun, J., Kennedy, B. C., Rosenfeld, S. S., ... and DeLaPaz, R. L., "Regression of recurrent malignant gliomas with convection–enhanced delivery of topotecan," Neurosurgery, vol 69, no. 6, pp. 1272–1280, 2011.

[7] Heiss, J. D., Jamshidi, A., Shah, S., Martin, S., Wolters, P. L., Argersinger, D. P., ... and Lonser, R. R., "Phase I trial of convection–enhanced delivery of IL13–Pseudomonas toxin in children with diffuse intrinsic pontine glioma," Journal of Neurosurgery: Pediatrics, vol 23, no. 3, pp. 333–342, 2018.

[8] Tanter, M., Pernot, M., Aubry, J. F., Montaldo, G., Marquet, F., and Fink, M, "Compensating for bone interfaces and respiratory motion in high–intensity focused ultrasound," International Journal of Hyperthermia, vol 23, no. 2, pp. 141–151, 2007.

[9] S. Jiménez–Gambén, N. Jiménez, J. M. Benlloch, and F. Camarena, "Holograms to focus arbitrary ultrasonic fields through the skull," Physical Review Applied, vol. 12, no. 1, p. 014016, 2019.

[10] A. N. Pouliopoulos, S.-Y. Wu, M. T. Burgess, M. E. Karakatsani, H. A. Kamimura, and E. E. Konofagou, "A clinical system for non-invasive blood–brain barrier opening using a neuronavigation-guided single–element focused ultrasound transducer," Ultrasound in medicine & biology, vol. 46, no. 1, pp. 73–89, 2020.

[11] U. Schneider, E. Pedroni, and A. Lomax, "The calibration of ct Hounsfield units for radiotherapy treatment planning," Physics in Medicine & Biology, vol. 41, no. 1, p. 111, 1996.

[12] T. D. Mast, "Empirical relationships between acoustic parameters in human soft tissues," Acoustics Research Letters Online, vol. 1, no. 2, pp. 37–42, 2000.

[13] R. S. Cobbold, Foundations of biomedical ultrasound. Oxford University Press, 2006.

[14] P. A. Yushkevich, J. Piven, H. C. Hazlett, R. G. Smith, S. Ho, J. C. Gee, and G. Gerig, "User–guided 3d active contour segmentation of anatomical structures: significantly improved efficiency and reliability," Neuroimage, vol. 31, no. 3, pp. 1116–1128, 2006.

[15] B. E. Treeby, and B. Cox, "Modeling power law absorption and dispersion for acoustic propagation using the fractional laplacian," The Journal of the Acoustical Society of America, vol. 127, no. 5, pp. 2741–2748, 2010.

[16] B. E. Treeby, J. Jaros, A. P. Rendell, and B. Cox, "Modeling nonlinear ultrasound propagation in heterogeneous media with power law absorption using a k-space pseudospectral method," The Journal of the Acoustical Society of America, vol. 131, no. 6, pp. 4324–4336, 2012.

Authorized licensed use limited to: UNIVERSIDAD POLITECNICA DE VALENCIA. Downloaded on November 30,2021 at 14:05:17 UTC from IEEE Xplore. Restrictions apply.